ELSEVIER

Journal of Power Sources 81–82 (1999) 442–447

JOURNAL OF POWER SOURCES

www.elsevier.com/locate/jpowsour

Lithium intercalation into and deintercalation from $Li_{1-\delta}Al_{1/4}Ni_{3/4}O_2$ electrode: current transient analysis

Su-Il Pyun *

Department of Materials Science and Engineering, Korea Advanced Institute of Science and Technology, 373-1 Kusong-Dong, Yusong-Gu, Taejon 305-701, South Korea

Abstract

The lithium intercalation into and deintercalation from $Li_{1-\delta}Al_{1/4}Ni_{3/4}O_2$ electrode was investigated by using current transient technique under large and small potential steps. From the fact that no potential plateau was observed in the charge–discharge curve, it was inferred that lithium-ion diffusion proceeds in a single phase of the electrode. The 'reduced' current build-up and decay transients upon the large potential stepping were analysed as compared with those current transients numerically simulated under the assumption of the simple finite-length diffusion. From the appearance of the current build-up and decay transients, it was suggested that the lithium transport through the electrode is mainly governed by the lithium ion diffusivity value during the lithium intercalation as well as deintercalation under the constant potential stepping. Also, the ratio of the transferred charge (Q_{int}/Q_{deint}) calculated from the measured current build-up and decay transients upon each small potential stepping was discussed in terms of cation mixing between the Ni^{3+} and Li^+ ions in the electrode.

Keywords: Lithium intercalation; $Li_{1-\delta}Al_{1/4}Ni_{3/4}O_2$ electrode; Current transient technique; Lithium-ion diffusion; Cation mixing

1. Introduction

There have been considerable research and development activity targeted towards the commercial manufacture of battery systems based on lithium intercalation materials [1–3]. This effort was primarily driven by the desire for inexpensive rechargeable lithium battery with high energy density which could be utilized in applications ranging in size from cellular phone and other electronic devices to electric vehicles.

Among the intercalation materials, the lithiated transition metal oxides such as $LiCoO_2$ [4], $LiNiO_2$ [5] and $LiNi_{1-y}Co_yO_2$ [6] have been intensively studied due to their very promising electrochemical performances. Although $LiNiO_2$ having a good reversibility is difficult to be synthesized, a great attention has been recently paid to $LiNiO_2$ due to its low cost and good charge retention compared with the first commercial material $LiCoO_2$ [7,8]. A convenient way to overcome the drawbacks of $LiNiO_2$ may be to use mixed phase with $LiAl_yNi_{1-y}O_2$ composition, because the presence of aluminium stabilizes the structure in a strictly two-dimensional fashion, thus favouring good reversibility and extended cycle life of $LiNiO_2$ [9].

Recently, the electrochemical lithium intercalation into transition metal oxides for rechargeable lithium battery system has been investigated by using current transient technique [10,11]. In particular, the current transients obtained from the $Li_{1-\delta}CoO_2$ electrode under the large and small potential steppings were quantitatively analysed in terms of the phase boundary, such material intrinsic properties as lithium ion diffusivity effect and extrinsic properties, e.g., electric field contribution [12]. Therefore, the analysis of current transient during the lithium intercalation and deintercalation gives us a better understanding of the lithium transport through the $LiAl_{1/4}Ni_{3/4}O_2$ electrode as an innovative rechargeable battery system.

The present work considers the lithium intercalation into and deintercalation from the $Li_{1-\delta}Al_{1/4}Ni_{3/4}O_2$ electrode by using X-ray diffractometry, galvanostatic charge–discharge experiment and current transient technique. From the current transients upon large and small potential steppings, the lithium transport through the electrode was discussed in view of lithium ion diffusion and cation mixing effect, respectively.

* Tel.: +82-42-869-3319; Fax: +82-42-869-3310; E-mail: sipyun@sorak.kaist.ac.kr

0378-7753/99/$ - see front matter
PII: S0378-7753(99)00228-1

2. Experimental

$LiAl_{1/4}Ni_{3/4}O_2$ powder was prepared by heating a pressed mixture of $LiNO_3$, $Al(OH)_3$ and $2NiCO_3 \cdot 3Ni(OH)_2 \cdot 4H_2O$ in stoichiometric proportions at 750°C for 24 h in air. The crystal structure of $LiAl_{1/4}Ni_{3/4}O_2$ was characterized by XRD. The powder XRD pattern was recorded on an automated Rigaku diffractometer using Cu Kα radiation. $LiAl_{1/4}Ni_{3/4}O_2$ electrode specimens were prepared by mixing $LiAl_{1/4}Ni_{3/4}O_2$ powder with 6 wt.% Vulcan XC-72 carbon black and 3 wt.% PVDF (polyvinylidene fluoride) in NMP (*n*-methyl pyrrolidone) solution. The stirred mixture was spread on Al-foil. Upon the evaporation of NMP the carbon-dispersed composite electrode specimens were dried under vacuum over 24 h. The exposed electrode area was 1 cm^2.

A three-electrode electrochemical cell was employed for the electrochemical measurements. The reference electrode as well as counter electrode was constructed from lithium foil (Foote Mineral, USA, purity 99.9%), and a 1M $LiClO_4$-propylene carbonate (PC) solution was used as the electrolyte.

Charge–discharge experiment was conducted under constant-current condition by using an EG&G PAR Model 263A potentiostat/galvanostat. The charge and discharge currents were selected so that a change in lithium content of $\Delta\delta = 1$ for $Li_{1-\delta}Al_{1/4}Ni_{3/4}O_2$ would occur for 5 h. Applying a constant current to the cell composed of the $Li_{1-\delta}Al_{1/4}Ni_{3/4}O_2$ electrode specimen, the resulting cell potential transients were recorded. The application of the constant current continued until the cell potential reached 4.2 V_{Li/Li^+}, after which we started to perform the measurement in the reverse direction, i.e., discharging, until the cell potential attained 3.0 V_{Li/Li^+}. Similar to the charge curve, the resulting cell potential transients were obtained. The deviation δ from the ideal stoichiometry of $LiAl_{1/4}Ni_{3/4}O_2$ was calculated from the values of the initial mass of the oxide and of the total transferred electrical charge during the whole charge–discharge cycles.

Two types of potentiostatic current transient experiments were performed by application of large potential steps (100 to 800 mV_{Li/Li^+}) and a small potential step (50 mV_{Li/Li^+}). The electrode was first polarized to the potential of 4.2 V_{Li/Li^+} for 5×10^3 s to obtain a low steady-state current and then the potentiostatic current build-up transients were measured by dropping 4.2 V_{Li/Li^+} to lithium injection potential in the potential range of 3.4 to 4.1 V_{Li/Li^+} in large steps during the lithium intercalation for 7×10^3 s. Subsequent potentiostatic current decay transients were made by jumping the lithium injection potential to 4.2 V_{Li/Li^+} in large steps during the lithium deintercalation for 10^4 s.

The potentiostatic current transients under the application of a small potential step were measured on the electrode. The electrode was first polarized to the potential of 3.4 V_{Li/Li^+} for 10^3 s to obtain a low steady-state current and then the potential was successively jumped by 50 mV_{Li/Li^+} for 1.2×10^4 s until the potential attained 4.2 V_{Li/Li^+}. From the moment just after each potential jump, the corresponding current decay transients were measured. The current build-up transients were obtained under the application of small potential drop (50 mV_{Li/Li^+}) in the reverse direction to 3.4 V_{Li/Li^+} in the same way as the build-up transients.

All electrochemical experiments were performed at 25°C in a glove box (MECAFLEX GB94) filled with purified argon gas.

3. Results and discussion

3.1. XRD characterization of $LiAl_{1/4}Ni_{3/4}O_2$

Fig. 1 shows the XRD pattern for $LiAl_{1/4}Ni_{3/4}O_2$ powder. All diffraction peaks can be indexed by assuming the structure to be a hexagonal lattice of the α-$NaFeO_2$ type to determine the lattice parameters $a = 2.86$, $c = 14.23$. The ideal layered $LiAl_{1/4}Ni_{3/4}O_2$ structure has a close-packed oxygen array which is slightly distorted from ideal cubic close packing. The trivalent aluminium and nickel ions are surrounded by six oxygen atoms forming $Al_{1/4}Ni_{3/4}O_2$ infinite slabs by edge-sharing of the $[Al_{1/4}Ni_{3/4}]O_6$ octahedra. The lithium ions are located between the $Al_{1/4}Ni_{3/4}O_2$ layers in octahedral sites. Therefore, the $LiAl_{1/4}Ni_{3/4}O_2$ phase has a rhombohedral structure with $R\bar{3}m$ space group and forms a solid solution of α-$LiAlO_2$($R\bar{3}m$) and $LiNiO_2$($R\bar{3}m$) by the ratio 1:3.

3.2. Galvanostatic charge–discharge curves for the $Li_{1-\delta}Al_{1/4}Ni_{3/4}O_2$ electrode

Fig. 2 presents the first to third galvanostatic charge–discharge curves obtained from the $Li_{1-\delta}Al_{1/4}Ni_{3/4}O_2$

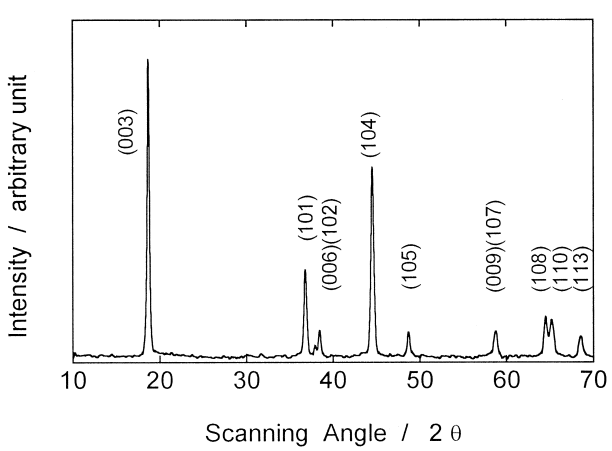

Fig. 1. X-ray diffraction pattern of $LiAl_{1/4}Ni_{3/4}O_2$. The Miller indices of the Bragg peaks are indicated over each peak.

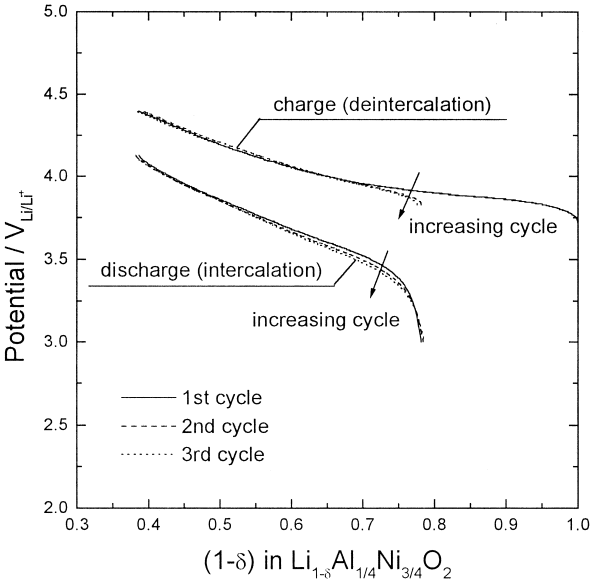

Fig. 2. First to third charge–discharge curves for the cell of Li/1 M $LiClO_4$-PC solution/$Li_{1-\delta}Al_{1/4}Ni_{3/4}O_2$ electrode. The change in lithium content, $\Delta\delta = 1$, for $Li_{1-\delta}Al_{1/4}Ni_{3/4}O_2$ occurs over 5 h.

electrode in 1 M $LiClO_4$-PC solution. No potential plateau was observed in the charge–discharge curve, indicating that the diffusion of lithium ion proceeds in a single phase of the electrode. Ohzuku et al. [13] reported that the charge–discharge curve obtained from the $LiNiO_2$ electrode shows three potential plateaux at 3.65, 4.00 and 4.20 V_{Li/Li^+} and Li et al. [14] found that those plateaux are due to the coexistence of two phases: hexagonal phase H1 and monoclinic phase M, phase M and hexagonal phase H2, and phase H2 and hexagonal phase H3, respectively. In particular, a noticeable capacity loss is caused by the formation of phase H3 during the lithium deintercalation above 4.20 V_{Li/Li^+} [13].

From the experimental finding that the potential plateau at 4.20 V_{Li/Li^+} did not appear on the charge–discharge curve shown in Fig. 2, it was expected that the capacity loss would not occur. However, the electrode suffers a capacity loss, 0.2 in lithium content $(1-\delta)$, during the first charge–discharge cycle, and it does not display more capacity loss during the following charge–discharge cycles. This is similar to the result reported by Arai et al. [15]: the irreversible capacity during the first charge–discharge cycle increases with the lithium deficiency z in the $Li_{1-z}Ni_{1+z}O_2$ electrode, indicating that the lithium intercalation is disturbed by the excessively substituted nickel in the lithium layer, i.e., occurrence of the cation mixing [8,16]. Therefore, the irreversibility in the first charge–discharge curve obtained from the $Li_{1-\delta}Al_{1/4}Ni_{3/4}O_2$ electrode is attributable to the lithium deficiency which is caused by the high vapour pressure of lithium at the calcination temperature. In order to examine in more detail the capacity loss due to the cation mixing during the first charge–discharge cycle, current transient experiment upon a small potential stepping was performed and the result will be discussed in Section 3.3.

3.3. Potentiostatic current transients for the $Li_{1-\delta}Al_{1/4}Ni_{3/4}O_2$ electrode

Let us first discuss about the lithium transport through the $Li_{1-\delta}Al_{1/4}Ni_{3/4}O_2$ asymmetric electrode under the impermeable boundary condition. Lithium atoms exist as lithium ions within the oxide electrode. Since during the lithium intercalation the space charge region can be generated nowhere within the oxide electrode, an electric field is not developed across the electrode. Thus, the lithium ion transport in the single-phase region can approximately be regarded as the lithium ion diffusion. When potentiostatic lithium injection into the $Li_{1-\delta}Al_{1/4}Ni_{3/4}O_2$ electrode is rate-controlled by lithium ion diffusion in the oxide electrode, the cathodic current can be expressed as a function of time, as Eq. (1) in the initial stage of diffusion and Eq. (2) in the later stage [17].

$$I(t) = \frac{Q\sqrt{\tilde{D}_{Li^+}}}{l\sqrt{\pi}}\frac{1}{\sqrt{t}}, \quad t \ll \frac{l^2}{\tilde{D}_{Li^+}} \tag{1}$$

and

$$I(t) = \frac{2Q\tilde{D}_{Li^+}}{l^2}\exp\left(-\frac{\pi^2\tilde{D}_{Li^+}}{4l^2}t\right), \quad t \gg \frac{l^2}{\tilde{D}_{Li^+}} \tag{2}$$

where $I(t)$ is the current as a function of time; Q, the total charge transferred during the lithium intercalation corresponding to the potential step $\Delta E(\int_0^\infty I(t)\mathrm{d}t)$; $\tilde{D}_{Li^+}$, the chemical diffusivity of lithium ion; l, the thickness of the electrode with planar symmetry and t represents the time. In the present work, we set the thickness l at the equivalent $R/3$ for the radius R of the spherical oxide particle. In the short time approximation, when $t \ll l^2/\tilde{D}_{Li^+}$, the chemical diffusivity $\tilde{D}_{Li^+}$ can be determined from the slope of the linear plot of I vs. $t^{-1/2}$. In the long time approximation, i.e., $t \gg l^2/\tilde{D}_{Li^+}$, the chemical diffusivity $\tilde{D}_{Li^+}$ can be evaluated from the slope of the semi-logarithmic plot of log I vs. t.

Fig. 3 illustrates current build-up transients for the simple diffusion in the electrode numerically simulated with various chemical diffusivities. The current transient for the simple diffusion shows a linear relationship between current and time in logarithmic scale with a slope of $-1/2$ in the initial stage, followed by a steep exponential decay with time in the later stage (two-staged transient). As the chemical diffusivity increased, the value of current density in the first stage increased and the time to a constant current density in the second stage was shortened.

In order to analyse the measured current transients upon large potential stepping in detail, the 'reduced' current was calculated as the measured current divided by total charge Q transferred into or from the $Li_{1-\delta}Al_{1/4}Ni_{3/4}O_2$ elec-

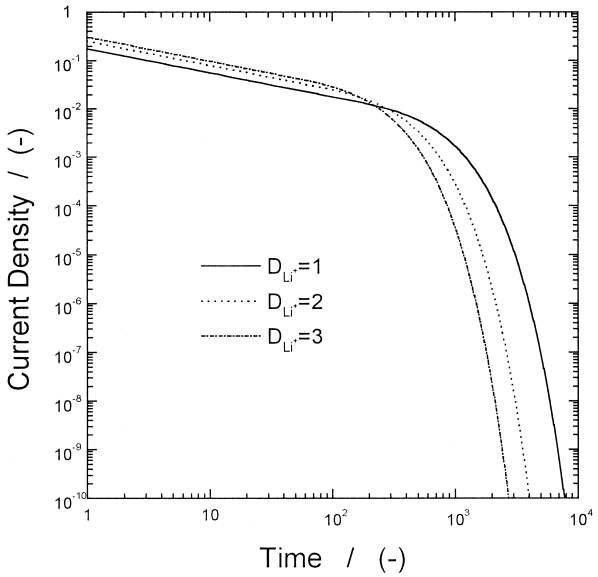

Fig. 3. Current build-up transients in logarithmic scale for the simple diffusion in the electrode numerically simulated with various chemical diffusivities.

trode at a given potential step during the lithium injection or extraction. The results are plotted against time (i/Q vs. time) in Fig. 4(a) and (b) in logarithmic scale. Fig. 4(a) and (b) demonstrate the current build-up and decay transients (reduced current vs. time) obtained from the electrode specimen in 1 M $LiClO_4$-PC solution at various lithium injection and extraction potential steps as indicated in the figures, respectively. Both the build-up and decay transients exhibited the two-staged behaviour with a constant slope of the first stage 0.1 to 0.3. The two-staged behaviour representing the simple finite-length diffusion is due to the lithium ion diffusion through the single phase in the oxide.

As the lithium injection potential decreased, the current value in the first stage decreased and the time to the constant current of 10^{-5} A in the second stage was prolonged. This behaviour is similar to that numerically simulated current transient. Recognizing that reduced current (i/Q) is strongly affected by the value of lithium ion diffusivity $\tilde{D}_{Li^+}$ as indicated in Eqs. (1) and (2), it is suggested that the chemical diffusivity of lithium ion is reduced with increasing lithium content, i.e., lowering lithium injection potential.

According to our previous work [12], the lithium transport through the $Li_{1-\delta}CoO_2$ electrode is mainly helped by the lithium ion diffusivity during the lithium intercalation, but it is mainly impeded by the electric field across the oxide electrode during the lithium deintercalation. During the lithium deintercalation from the $Li_{1-\delta}CoO_2$ electrode, the electronic potential gradient is developed across the electrode due to the metallic conductivity of $Li_{1-\delta}CoO_2$ at low lithium content. In contrast, since the $Li_{1-\delta}Al_{1/4}Ni_{3/4}O_2$ has an insulating conductivity at low lithium content [9], the effect of the electric field on the lithium transport can be disregarded during the lithium deintercalation as well as intercalation.

In order to explore in detail the cation mixing effect mentioned in Section 3.2, the charges transferred Q_{int} and Q_{deint} during the lithium intercalation and deintercalation were calculated from the corresponding build-up and decay transients upon each small potential dropping and jumping, respectively. Fig. 5 depicts the plot of the ratio of the transferred charge (Q_{int}/Q_{deint}) calculated from the current transients upon the small potential dropping and

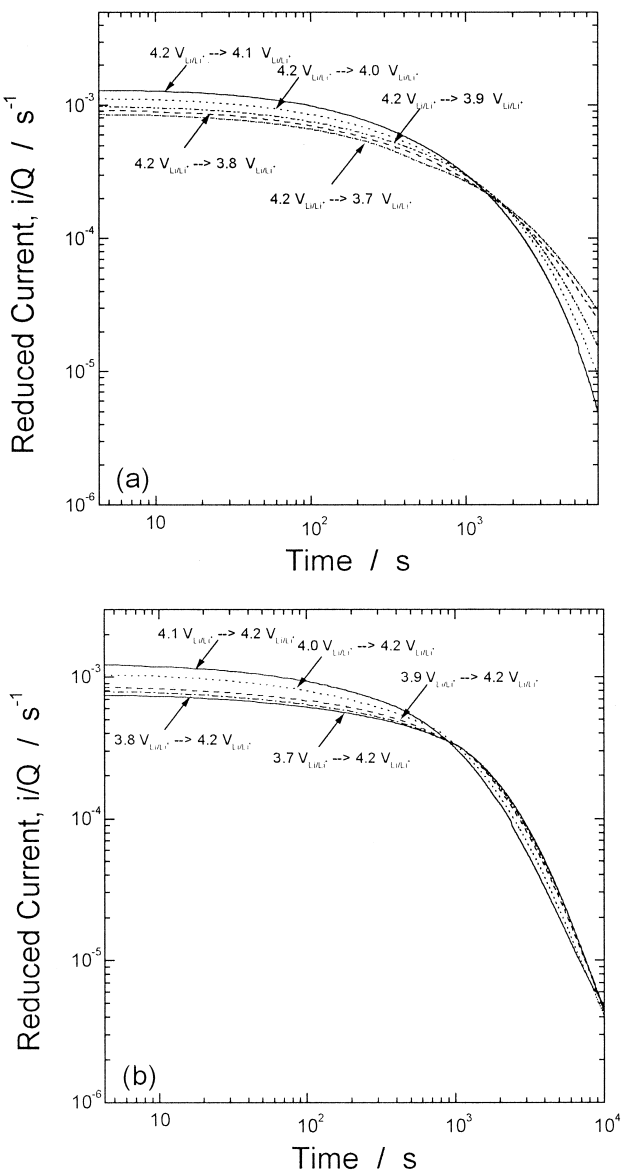

Fig. 4. (a) Reduced current build-up and (b) decay transients in logarithmic scale, obtained from the $Li_{1-\delta}Al_{1/4}Ni_{3/4}O_2$ electrode in 1 M $LiClO_4$-propylene carbonate solution. Lithium was injected into the electrode by dropping 4.2 V_{Li/Li^+} to various lithium injection potentials as indicated in the figures and the lithium extraction was followed by jumping the lithium injection potential to 4.2 V_{Li/Li^+}.

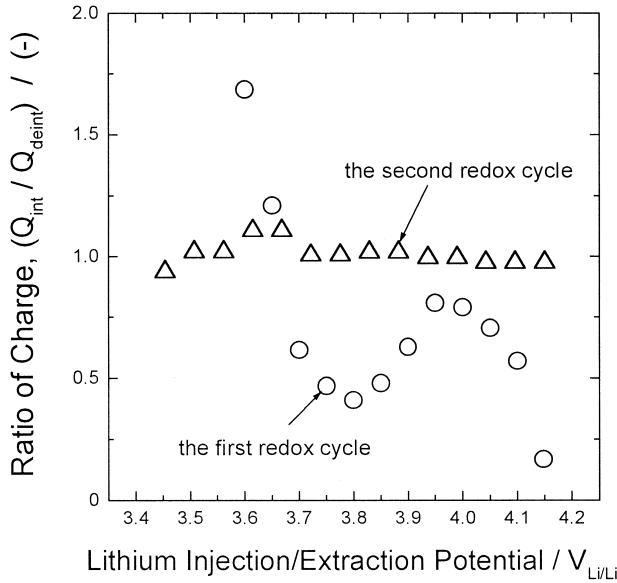

Fig. 5. Plot of the ratio of the transferred charge (Q_{int} / Q_{deint}) vs. lithium injection and extraction potentials during the 1st (○) and 2nd (Δ) redox cycles. The charges Q_{int} and Q_{deint} were calculated from the measured build-up and decay transients of the $Li_{1-\delta}Al_{1/4}Ni_{3/4}O_2$ electrode, respectively, under the application of each small potential step (50 mV_{Li/Li^+}).

jumping against lithium injection and extraction potentials, respectively, during the first and second redox cycles. Assuming that the transferred charge is entirely consumed by the lithium intercalation into and deintercalation from the electrode, the charge ratio should be unity, i.e., it follows the Faraday law.

In fact, the charge ratio markedly deviated from unity in value over the whole injection/extraction potential range during the first redox cycle, but that ratio value approached almost unity over the whole potential range during the second redox cycle. It is worthwhile to note that the cation mixing effect can be rated as degree of the reversibility between the lithium intercalation into and deintercalation from the electrode. Therefore, the strong deviation of the ratio value from unity is due to the cation mixing between the Ni^{3+} and Li^+ ions in the oxide electrode. In Figs. 2 and 5 the irreversibility in the capacity was almost entirely completed during the first cycle, and hence it did not appear any more during the second and further following cycles. This means that substitutive aluminium stabilized the layered structure, thus the formation of H3 was suppressed during the prolonged charge–discharge cycle. In contrast, the theoretical capacity of the $Li_{1-\delta}Al_yNi_{1-y}O_2$ electrode decreases with increasing aluminium content y. Therefore, the optimization of aluminium content and the detailed investigation of the effect of aluminium content on the cation mixing are strongly needed for favouring good reversibility and extended cycle life. Such developments are under progress in our laboratory.

4. Conclusions

The present work is concerned with the lithium intercalation into and deintercalation from the $Li_{1-\delta}Al_{1/4}Ni_{3/4}O_2$ electrode. From the experimental results, the following conclusions are drawn.

(1) No potential plateau was observed in the charge–discharge curve, indicating that lithium-ion diffusion proceeds in a single phase of the electrode. The irreversible capacity during the first charge–discharge cycle indicates that the lithium intercalation is disturbed by the cation mixing between the Ni^{3+} and Li^+ ions in the oxide electrode.

(2) The 'reduced' current build-up and decay transients measured under the large potential stepping were similar to those current transients numerically simulated on the condition of the simple-finite length diffusion only as a function of chemical diffusivity. From the appearance of the 'reduced' current build-up and decay transients, it was concluded that the chemical diffusivity of lithium ion mainly contributes to the lithium transport through the oxide electrode during the lithium intercalation and deintercalation.

(3) The ratio of the charge transferred during the intercalation Q_{int} to that charge during the deintercalation Q_{deint} calculated from the corresponding build-up transient and decay transient upon each small potential dropping and jumping, respectively, is regarded as degree of reversibility between the lithium intercalation into and deintercalation from the electrode. The value of the charge ratio markedly deviates from unity during the first redox cycle, but it maintains nearly unity just satisfying the Faraday law during the second redox cycle. This means that the irreversibility in the capacity has almost completely operated during the first redox cycle, and therefore, no cation mixing occurs more during the second redox cycle.

Acknowledgements

The receipt of research grant under the programme 'Development of technology of high performance batteries for electric vehicle application 1997/1998' from the Ministry of Commerce and Industry, Korea is gratefully acknowledged. Incidentally the Ministry of Information and Communication, Korea financially supported this work under the university foundation research programme 'Development of High Performance Rechargeable Lithium Battery for Telecommunication Application 1997/1998'. The author is deeply indebted to Mr. S.-W. Kim and M.-H. Lee, Korea Advanced Institute of Science and Technology (KAIST), for their helpful discussion. It is noted that Mr. Y.-M. Choe, KAIST, made start aid for preparing this manuscript during his stay at KAIST in the period of 1997/1998.

References

[1] M.S. Whittingham, J. Electrochem. Soc. 123 (1976) 315.
[2] S. Atlung, K. West, T. Jacobsen, J. Electrochem. Soc. 126 (1979) 1311.
[3] D.W. Murphy, P.A. Christian, Science 205 (1979) 651.
[4] K. Mizushima, P.C. Jones, P.J. Wiseman, J.B. Goodenough, Mater. Res. Bull. 15 (1980) 783.
[5] J.R. Dahn, U. von Sacken, C.A. Michal, Solid State Ionics 44 (1990) 87.
[6] C. Delmas, I. Saadoune, Solid State Ionics 53 (1992) 370.
[7] W. Ebner, D. Fouchard, L. Xie, Solid State Ionics 69 (1994) 238.
[8] Y.-M. Choi, S.-I. Pyun, S.-I. Moon, Y.-E. Hyung, 72 (1998) 83.
[9] T. Ohzuku, A. Ueda, M. Kouguchi, J. Electrochem. Soc. 142 (1995) 4033.
[10] J.-S. Bae, S.-I. Pyun, Solid State Ionics 90 (1996) 251.
[11] S.-I. Pyun, Y.-M. Choi, J. Power Sources 62 (1997) 524.
[12] Y.-M. Choi, S.-I. Pyun, J.M. Paulsen, Electrochim. Acta 44 (1998) 623.
[13] T. Ohzuku, A. Ueda, M. Nagayama, J. Electrochem. Soc. 140 (1993) 1862.
[14] W. Li, J.N. Reimers, J.R. Dahn, Solid State Ionics 67 (1993) 123.
[15] H. Arai, S. Okada, H. Ohtsuka, M. Ichimura, J. Yamaki, Solid State Ionics 80 (1995) 261.
[16] Y.-M. Choi, S.-I. Pyun, S.-I. Moon, Solid State Ionics 89 (1996) 43.
[17] J. Crank, in: The Mathematics of Diffusion, Clarendon Press, Oxford, 1975, p. 286.